

Compositing Ground Penetrating Radar Scans of Differing Frequencies for Better Depth Perception

Roger Tilley, Hamid R. Sadjadpour, Farid Dowla

Department of Electrical Engineering
University of California, Santa Cruz
Santa Cruz, CA. 95064

Email: {rtvax, hamid, dowla} @soe.ucsc.edu

Abstract— Methods developed to reduce interference in a noisy environment, be it radar target responses or effective communications in the presence of noise for mobile phone users, are vital in delivering a clear usable signal. The methods used to render a cleaner signal can also be used to combine signals of various frequencies. Ground Penetrating Radar (GPR) scans over the same area are no exception. This paper explores using an optimization problem solver, the Expectation Maximization (EM) Algorithm, to define the weights to use to combine multiple GPR scans at different frequencies over the same target area. This approach exploits the Gaussian Mixture Model (GMM) feature of the EM algorithm to produce a cleaner image at depth. Our method demonstrates a measured improvement toward producing a cleaner image.

Keywords— Ground Penetrating Radar; Expectation Maximization; Gaussian Mixture Model; Maximum Likelihood parameter estimation; Finite Difference Time Domain Method, GprMax.

I. INTRODUCTION

Ground Penetrating Radar (GPR) scans are used to illuminate objects in various terrain types at different depths. The frequency scan that best illuminates an object is different at each depth. Higher frequency scans image objects closer to the surface in great detail while lower frequencies image objects deeper with less fidelity. Assuming GPR radar scans at different frequencies over the same terrain can be treated like sub-components of a square wave, where the summation of sub-components determines a crisp square wave; then, adding the scans together should form an improved image of the terrain being scanned with higher resolution to a lower depth [1]; a byproduct of the summation. Just simply adding each scan together, as demonstrated in this paper, has been shown not to be sufficient for the GPR case but does suffice for square wave, triangle wave, and sawtooth wave cases. For GPR scans, a weighted version of each scan presents the best solution to this problem [2]. Employing an optimization problem solver to determine the weight applied to each scan is the first use of this method to develop an optimal weighted combination of GPR frequency scans. In the literature, other methods have been proposed to solve this problem with varying success; all with a very similar approach to each other. Methods by Dougherty et al. [3], Booth et al. [4], and

Bancroft [5] all discussed ways to weight each signal used to combine individual frequency traces of GPR scans. Absent from these works are optimization problem solvers such as the Expectation Maximization (EM) Algorithm [6]. We have chosen to investigate using the data mixture feature of the EM Algorithm to develop optimal weights.

In this paper, we describe the EM algorithm and its data mixture feature, as it relates to GPR scans of different frequencies, and compare the results with the methods of Dougherty et al. [3], Booth et al. [4], and Bancroft [5]. This paper is organized as follows. In Section II, we discuss work related to the multi-frequency GPR mixture process. In Section III, the EM Algorithm data mixture process is described. In Section IV, the Maximum-Likelihood (ML) Estimation process and its relationship to the EM Algorithm data mixture process [6][7] is described. In Section V, we present an EM Algorithm Test Case. Section VI, briefly, describes the methods of Dougherty et al. [3]. In developing signal weights. Section VII, the methods examined by Booth et al. [4] are discussed. In Section VIII, the methods proposed by Bancroft [5] are discussed. In Section IX, we demonstrate that computer modeling can be used to substitute for real data. In Section X, we present results of simulated GPR scan examples using the software GprMax [8], comparing EM Algorithm data mixture method with methods of Dougherty et al. [3], Booth et al. [4], and Bancroft [5]. In Section XI, we draw some conclusions and discuss possible future work.

II. RELATED WORK

A search of the relevant literature uncovered only a few publications on compositing of GPR signals. The earliest works found discussed GPR time-slice analysis, GPR overlay analysis and GPR isosurface rendering, all similar in approach; mostly by archaeologists. The general approach was to illuminate the strongest reflections at a specified time or depth with a color or shading. Assemble the information by layers of depth or time and display the completed result. [9].

Dougherty et al. [3] was the earliest work found, which attempted to combine GPR signal traces for site characterization and bandwidth enhancement. Their

research involved real data taken from a former lumber mill waste site near Boise, Idaho. Part of the focus was on developing a method to simulate the direct arrival pulse to ultimately subtract from the traces. An additional paper focus was on enhancing the GPR response by summing the traces of differing frequencies. The latter part of the paper, focused on establishing proof of bandwidth enhancement through summation. Some success was noted but, equally weighting and summing the traces only marginally enhanced the results. Bandwidth enhancement was confirmed after trace summation using correlation.

The results of Dougherty et al. [3] were re-affirmed in two publications both authored by Booth et al. [2][4]. They successfully repeated the enhancement of the spectral bandwidth by compositing; adding to the compositing method, shifts to align trace direct arrival peaks and an adjustment to trace weights before summing. The scan weights were adjusted to enhance the magnitude of the higher frequency scans while de-emphasizing the magnitude of lower frequency scans. Booth et al. [2] used data sets from glacial deposits near Guelph, Ontario, Canada for the first publication. The second publication [4], focused on attempting to find the best method to combine GPR frequency scans. GPR data sets from the Waterloo Moraine in Ontario, Canada were analyzed. Several methods to combine multiple frequencies were documented. Weighting factors were developed from trace averaged amplitude spectra, as well as time invariant weighting factors output from a least-squares analysis, were evaluated. The time invariant weight methods developed, attempted to match the compositing results to an idealized amplitude spectrum. Improvements over Dougherty et al. [3], were realized.

Bancroft [5] continued the work by studying previous compositing methods by Dougherty et al. [3], and Booth et al. [4]. Bancroft [5] introduced additional methods to compute weights for use in compositing GPR frequencies. One introduced method Bancroft [5] named the double ramp summation method, where one ramp suppresses a frequency's energy over time while a second ramp introduces an adjacent frequency's energy over time. The ramp length was arbitrarily defined but, based on the wavelength of the GPR frequency of interest. The start time for each ramp was a calculated value based on the GPR frequency of interest. Bancroft's [5] other method was called Amplitude Envelope Equalization. The weights used in this ramp summation technique were developed as a ratio of the average envelope of GPR frequencies. Improvements over Booth et al. [4] were not dramatic for the cases presented.

The "state of the art" or related work to date has focused on mathematically defining the weights for each frequency by equal weighting, by the value needed to equalize the spectra of GPR frequencies, through ramp summation, or by a least-squares process to match an idealized amplitude spectrum. Optimization problem solving methods have yet to be explored. Our previous work [1] addresses the

problem as a clustering mixture model problem, well suited for EM methods.

III. EXPECTATION MAXIMIZATION ALGORITHM

The EM Algorithm is used to solve many types of problems. One type is to group like items contained in complex mixtures; another type is to solve incomplete data problems by performing Maximum Likelihood (ML) parameter estimation. A third type is to determine the membership weights of data points in a cluster within a finite Gaussian Mixture Model (GMM) [10][11]. This third feature is what will be exploited to combine multiple GPR frequency scans into a composite wave. Other mathematical distributions can represent the data set created by GPR scans, but we used a Gaussian distribution because it is often used when the distribution of the real-valued random variables is unknown.

We can define a finite mixture model $f(\underline{x};\theta)$ of K components as mixtures of a Gaussian function as:

$$f(\underline{x};\theta) = \sum_{k=1}^K \alpha_k p_k(\underline{x} | \theta_k), \quad (1)$$

Where:

- $p_k(\underline{x} | \theta_k)$ are K mixture components with a distribution defined over $p(\underline{x} | \theta_k)$ with parameters $\theta_k = \{\underline{\mu}_k, C_k\}$ (mean, covariance)
- $p_k(\underline{x} | \theta_k) = \frac{1}{(2\pi)^{d/2} |C_k|^{1/2}} e^{-\frac{1}{2}(\underline{x}-\underline{\mu}_k)^T C_k^{-1}(\underline{x}-\underline{\mu}_k)}$ (2)
- α_k are K mixture weights, where $\sum_{k=1}^K \alpha_k = 1$.
- $\{\underline{x}_1, \dots, \dots, \underline{x}_n\}$ Data set for a mixture component in d dimensional space.

There are 2 steps in each iteration of the EM Algorithm, the Expectation step (E-step) and the Maximization step (M-step). The E-Step computes the conditional expectation of the group membership weights (w_{ik} 's) for \underline{x}_i 's, adding unobservable data given θ_k . The M-Step computes new parameter values ($\alpha_k, \underline{\mu}_k, C_k$) to maximize the finite mixture model using the membership weights. The E-Step and M-Step are repeated until a stopping criterion is reached (convergence). Convergence is indicated by the log-likelihood of $f(\underline{x};\theta)$ not changing substantially from one iteration to the next.

E-Step –

$$w_{ik} = \frac{p_k(\underline{x}_i | \theta_k) \alpha_k}{\sum_{m=1}^K p_m(\underline{x}_i | \theta_m) \alpha_m} \quad (3)$$

for $1 \leq k \leq K, 1 \leq i \leq N$;

with constraint $\sum_{k=1}^K w_{ik} = 1$

M-Step –

$$N_k = \sum_{i=1}^N w_{ik} \quad (4)$$

$$\alpha_k^{new} = \frac{N_k}{N}, \text{ for } 1 \leq k \leq K \quad (5)$$

$$\underline{\mu}_k^{new} = \left(\frac{1}{N_k}\right) \sum_{i=1}^N w_{ik} * \underline{x}_i \quad (6)$$

for $1 \leq k \leq K$

$$C_k^{new} =$$

$$\left(\frac{1}{N_k}\right) \sum_{i=1}^N w_{ik} * \left(\underline{x}_i - \underline{\mu}_k^{new}\right) \left(\underline{x}_i - \underline{\mu}_k^{new}\right)^T \quad (7)$$

Convergence (log likelihood of $f(\underline{x}; \theta)$) –

$$\text{Log } l(\vartheta) =$$

$$\sum_{i=1}^N \log f(\underline{x}_i; \theta) =$$

$$\sum_{i=1}^N \left(\log \sum_{k=1}^K \alpha_k p_k(\underline{x}_i | \theta_k)\right) \quad (8)$$

These equations that make up the EM Algorithm were implemented in MATLAB. The variables ‘k’ and ‘x’ represent the different scanning frequencies and GPR trace scans, respectively. Each trace, at a frequency and transmitter (Tx)/receiver (Rx) position, are analyzed and combined for all frequencies using the EM Algorithm before moving on to the next position. Described below are the EM GMM process steps.

Expectation Maximization Gaussian Mixture Model process:

1. Initialize algorithm parameters; weights (mixture and group membership), mean, covariance, for each trace.
2. Expectation step – estimate parameters.
3. Maximization step – maximize estimated parameters.
4. Check for convergence – log likelihood of mixture model.
5. Repeat steps 2 – 4 until change from iteration to iteration is below or equal a defined value.
6. Combine traces with defined mixture weights.

IV. MAXIMUM LIKELIHOOD ESTIMATION PROCESS AND THE EM RELATIONSHIP

Maximum Likelihood Estimation (MLE) can provide a good estimate of an unknown parameter, which maximizes the probability of getting the data we observed (likelihood). A simple example is as follows. Given a random sample X_1, X_2, \dots, X_n , independent and identically distributed (i.i.d.) with a probability density function $f(x_i, \theta)$, where θ is the unknown parameter to be estimated; the joint probability density function (PDF) can be labeled as $L(\theta)$.

$$L(\theta) = P(X_1 = x_1, X_2 = x_2, \dots, X_n = x_n) = f(x_1; \theta) * f(x_2; \theta) \dots f(x_n; \theta) = \prod_{i=1}^n f(x_i; \theta) \quad (9)$$

Assuming the probability density function is Gaussian with known variance σ^2 and unknown mean, μ , then, the likelihood equation becomes the following:

$$L(\mu) = \prod_{i=1}^n f(x_i; \mu, \sigma^2) = \sigma^{-n} (2\pi)^{-n/2} \exp\left(-\frac{1}{2\sigma^2} \sum_{i=1}^n (x_i - \mu)^2\right) \quad (10)$$

To solve for the mean, μ , we take the partial derivative of the log likelihood equation with respect to (w.r.t.) the mean, μ , and set the result equal to 0 to solve the resultant equation for the variable μ . Taking a second partial derivative of the log likelihood w.r.t. μ and returning a negative value verifies that the parameter μ does indeed represent the maximum value for the likelihood function.

$$\text{Log } (L(\mu)) = -n \log(\sigma) - \frac{n}{2} \log(2\pi) - \sum_{i=1}^n \frac{(x_i - \mu)^2}{2\sigma^2} \quad (11)$$

$$\frac{\partial}{\partial \mu} (\log(L(u))) = -2(-1) \sum_{i=1}^n \frac{(x_i - \mu)}{2\sigma^2} = 0 \quad (12)$$

$$\text{Solve for } \mu; \quad \mu = \frac{\sum_{i=1}^n x_i}{n} \quad (13)$$

The process can be repeated for the variance should it not be known. The MLE process becomes hard if there are at least two sets of data where only one set is partially observed (hidden) or when estimating mixture parameters is necessary.

A mixture distribution has a PDF of the form $f(x) = \sum_{k=1}^K \alpha_k f(x; \theta_k)$, where there are K number of components in the mixture model and for each k, there is a PDF, $f(x; \theta_k)$ as well as a weight α_k and a complete observed data set x. Other assumed constraints are $\sum_k \alpha_k = 1$ and $\alpha_k \geq 0$ for all k. The joint PDF takes on the form with n observed data for each k:

$$L(x|\alpha, \theta_k) = \prod_{i=1}^n \sum_{k=1}^K \alpha_k f(x_i; \theta_k) \quad (14)$$

The log of the likelihood equation yields the following:

$$\text{Log}((L(x|\alpha, \theta_k))) = \sum_{i=1}^n \log \sum_{k=1}^K \alpha_k f(x_i; \theta_k) \quad (15)$$

Solving this weighted MLE equation using MLE is challenging because of the log of sums and the challenge to determine what value to start with for the weight associated with an individual distribution α_k . There may be many local maxima that are less than the global maximum that are available. Choosing the weight value that arrives at the global maximum for the log likelihood is not likely in short order.

The EM algorithm provides a means to estimate the weights and guarantee convergence of the likelihood equation [6][7] to a non-decreasing local maximum with each completion of all steps of the algorithm. The EM algorithm reduces the MLE optimization problem to a sequence of simpler optimization sub-problems that are each guaranteed to converge.

Another way to describe the MLE process and the EM algorithm relationship is through this example of 2 different coins tossed [12]. Two coins each tossed 10 times with the result of Heads or Tails recorded as well as, which coin produced the recorded values for 5 sets of 10 tosses. All information is known therefore the calculation of the probability of Heads (θ_A) for coin A and the calculation of Heads (θ_B) for coin B are straight forward.

$$\theta_A = \frac{\text{\#of heads using coin A}}{\text{Total \# of coin flips for coin A}} \quad (16)$$

$$\theta_B = \frac{\text{\#of heads using coin B}}{\text{Total \# of coin flips for coin B}} \quad (17)$$

Restructuring the problem such that the coin that was used, for any of the 5 sets of 10-coin tosses, is unknown. The approach of calculating with hidden data, which coin, involves an iterative scheme where a guess is made to determine, which coin was used for each of the 5 sets; then, calculating the MLE as before; repeating this process until convergence. Many local maxima are found before the global maximum is determined. Each local maximum reached in the interim is not necessarily larger than the previous outcome. Changing the initial guess can change the order of the outcome.

The EM process for this example is implemented such that the probability of start values is calculated using existing data (Expectation Step). The following step is to recalculate the model parameters then, calculate the maxima for that set of parameters using an MLE process (Maximization Step). The EM process is repeated until a global maximum is reached. The EM process creates a simpler optimization sub-problem at each iteration that is guaranteed to converge and has been shown to have an increasing maximum value for each cycle (E-Step, M-Step). A set of equations as shown below represent the EM solution given initial values of θ_A and θ_B .

Expectation Step

$$p(A)_i = \frac{\theta_A^{NH} (1-\theta_A)^{NH}}{\theta_A^{NH} (1-\theta_A)^{NH} + \theta_B^{NH} (1-\theta_B)^{NH}} \quad (18)$$

$$p(B)_i = \frac{\theta_B^{NH} (1-\theta_B)^{NH}}{\theta_A^{NH} (1-\theta_A)^{NH} + \theta_B^{NH} (1-\theta_B)^{NH}} \quad (19)$$

where: NH is the number of heads in set i of 5 sets of 10 tossed coins, x_i ;

$p(A)_i$ – probability of heads for coin A in set i ;

$p(B)_i$ – probability of heads for coin B in set i

Maximization Step

$$\theta_A = \frac{\sum_{i=1}^5 p(A)_i}{\sum_{i=1}^5 p(A)_i + \sum_{i=1}^5 p(B)_i} \quad (20)$$

$$\theta_B = \frac{\sum_{i=1}^5 p(B)_i}{\sum_{i=1}^5 p(A)_i + \sum_{i=1}^5 p(B)_i} \quad (21)$$

The EM algorithm provides a workable solution to a very hard problem when hidden or incomplete data exists. It incorporates the MLE process only after reducing the model to a form, which is guaranteed to converge. Combining GPR

frequency scans have an aspect that the actual weight values for each frequency are unknown or hidden. The way the EM algorithm accomplishes workable solutions to hidden or incomplete data sets, distinguishes it from other optimization problem solvers, thus making it a featured candidate to provide a viable solution for combining multiple GPR frequency scans.

V. EXPECTATION MAXIMIZATION TEST CASE

As an EM GMM test case, we constructed a series of six sine waves (50, 150, 250, 350, 450 and 550 Hz) noted in Figures 1-3, which when weighted properly, sum to the square wave of Figure 4. Figure 5, demonstrates the result determined by the EM GMM as compared to the desired result. The apparent error can be attributed to at least two conditions; to machine round off errors of the computer used and to the group membership weights, w_{ik} and/or mixture weights, α_k each constrained to sum to one. The weights normally sum to greater than one depending on the number of signals added together. Even when the weights for sine wave to square wave construction are scaled to a maximum value of one; they still do not match up to the EM GMM generated weights. Despite this limitation, the mixed success

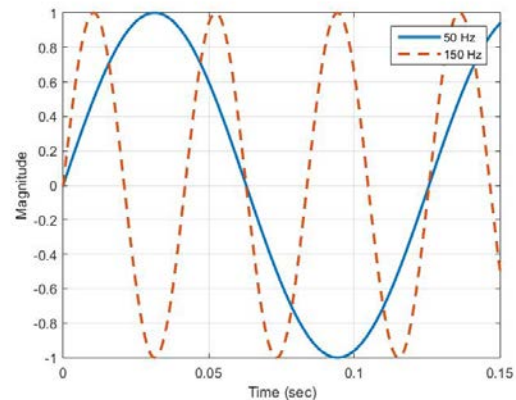


Figure 1. Sine wave frequencies 50-150 Hz.

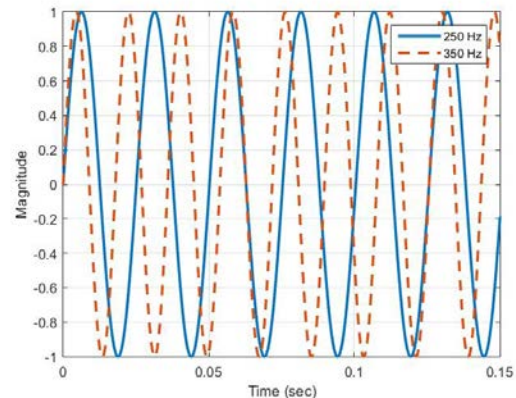


Figure 2. Sine wave frequencies 250, 350Hz.

of adding arbitrary frequencies together bolsters our idea to use the EM GMM method on multiple GPR scans. The GPR frequencies to choose for the analyses are simply the frequencies needed to span the depth and detail the GPR user wishes to achieve. As a reminder, low frequencies image deep with low resolution where as high frequencies image with great detail in a shallow area.

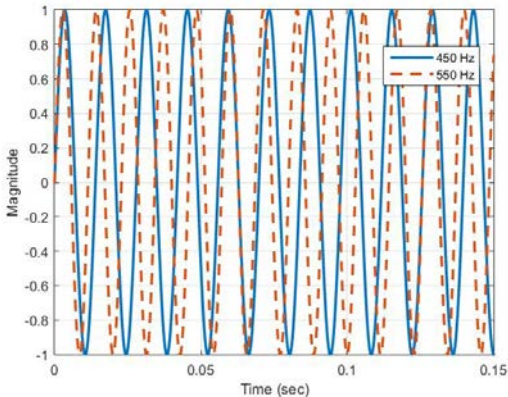


Figure 3. Sine wave frequencies, 450-550 Hz.

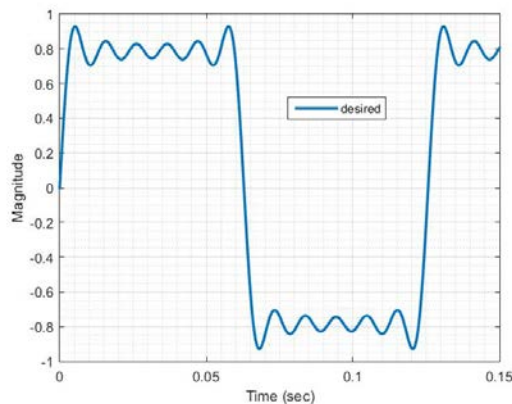


Figure 4. Square wave desired signal.

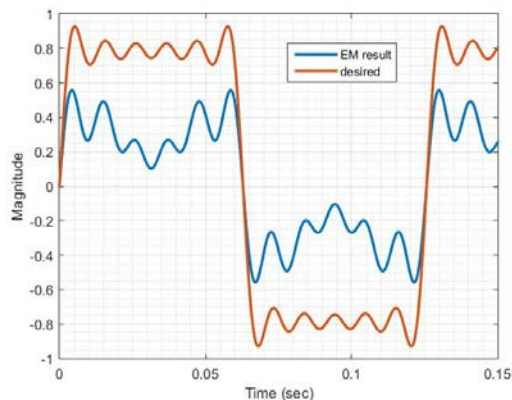


Figure 5. EM algorithm result with desired signal.

VI. DOUGHERTY ET AL. PROCESS

Dougherty et al. [3], collected GPR data from a former lumber mill waste site near Boise, Idaho. He sought to enhance the original GPR data through air wave/direct arrival wave removal, and bandwidth enhancement. They first aligned each trace by the direct arrival pulse in each trace then, removed DC shifts; the low frequency “wow” component, followed by scaling each trace by the L2 norm of the direct arrival pulse. The traces were summed and the resultant direct arrival estimate was then, subtracted from each trace removing the direct arrival signal. An exponential gain recovery function was applied to each trace. Equal weighting was applied to each trace with the direct arrival signal removed as each frequency was summed. Dougherty et al. [3] demonstrated some clarity of shallow reflections due to direct wave removal. They achieved resolution and continuity of reflection enhancement by summing the frequencies. Spectral bandwidth was increased as well. However, the resultant signal was overwhelmed by the lower frequencies in the summation.

Dougherty et al. [3] process steps are as follows:

1. Align each trace by direct arrival.
2. Remove DC shift.
3. Remove low frequency (wow).
4. Scale each trace by L2 norm of direct arrival pulse.
5. Sum traces to form estimate of direct arrival signal.
6. Subtract estimate from each trace.
7. Apply exponential gain recovery function
8. Apply equal weighting to each trace.
9. Sum each trace all frequencies.

VII. BOOTH ET AL. PROCESS

Booth et al. [4], using real data acquired at a site on the Waterloo Moraine (an accumulation of glacial debris) in Ontario, Canada, examine five methods of achieving an increased bandwidth and thus a more approximate delta function through evaluating composite synthetic GPR wavelets; with a few method variations. The simple summation of [3] was examined, as one method. A second method, examined a scaled summation approach where the maximum value of each frequency spectra was determined and the spectrums equalized. The values used to equalize the spectra provided the signal weighting prior to summation. A third method, involved shifting traces such that the main peaks of the direct arrival pulses were aligned with the dominant peak then, the scaled summation of method two was applied. Method three provided the best result for increased spectral bandwidth, thus the best delta function, and GPR resolution for synthetic wavelets. Booth et al. [4] repeated the above analyses with GPR traces with one change. The time-shifting of traces was changed to align the first break of each trace at 0 ns. Then method two was applied, averaging the frequency spectra of each trace for one frequency then, determining the frequency weight;

repeating for all frequencies. This process was given the name of dominant frequency amplitude equalization (DFAE). As a final discussion, another weighting method was examined where the weighting factors were obtained from a least squares analysis, Optimal Spectral Whitening (OSW) that attempts to match the summed result to a defined optimal amplitude spectrum. The defined optimal spectrum determines over what set of frequencies the frequency data sets would be enhanced. A time-varying Fourier transformation of each data set must be performed prior to implementing the least square analysis.

The OSW process determined a time window to operate on by choosing the longest wavelet period of the GPR scanned frequencies. A frequency spectrum was produced for each time window of each trace. The spectra for a scan frequency were averaged together, and a magnitude was determined for each scanned frequency over the time-window spectra. The magnitude determined became a row in the OSW matrix. The process continues for each scan frequency for that time-window resulting in an over-determined linear system. Then solving the over-determined linear system for the frequency weights using a defined desired spectral amplitude. The desired spectral amplitude is usually defined as identical values (constant), one for each scan frequency. The OSW process is complete with the combining of traces for that time window with the computed weights.

Booth et al. [4] process steps are as follows:

Method 2 –

1. Determine frequency spectrum of each wavelet.
2. Equalize spectra for all frequencies; the magnitude needed to equalize spectra determines the weight for that frequency. (method 3 variation – average the frequency spectra of each trace for one frequency then, determining the weight; repeating for all frequencies).
3. Sum each wavelet of all frequencies with appropriate weight for that frequency.

Method 3 –

1. Shift all traces such that main peaks of Direct Arrival Signal are aligned. (variation – align the first break of each trace to 0 ns).
2. Continue by applying the steps of method 2.

DFAE – method 4

1. Remove DC shift.
2. Remove low frequency (wow).
3. Shift all traces to first break of Direct Arrival.
4. Remove direct signal (mute-ramping from 0% to 100% at chosen mute time).
5. Determine frequency spectrum of each trace.
6. Average spectrum for ensemble estimate.
7. Equalize ensemble spectra for all frequencies; the magnitude needed to equalize spectra determines the weight for that frequency.

8. Sum each trace of all frequencies with appropriate weight for that frequency.

OSW – method 5

1. Remove DC shift.
2. Remove low frequency (wow).
3. Shift all traces to first break of Direct Arrival.
4. Remove direct signal (mute- mute-ramping from 0% to 100% at chosen mute time).
5. Average traces for each frequency.
6. Compute spectra of average trace for each frequency.
7. Determine magnitude at scan frequencies for each spectra; becomes a row in OSW matrix “A”. One row for each frequency.
8. Determine idealized frequency spectra vector “S”; vector usually set to value of one for each scan frequency.
9. Determine weights by solving matrix equation $W = (A^T * A)^{-1} * A^T * S$.
10. Combine weighted frequency traces; $sum = traces * W$.
11. Repeat steps 6 -10 for all analysis time windows over the GPR reflection Profile. Time window should be greater than the longest wavelet period to be sampled.

VIII. BANCROFT PROCESS

Bancroft [5], using real data from Santa Rosa Island, Florida, discusses the findings of Dougherty et al. [3] and the methods described by Booth et al. [4], while defining other methods to determine the weighting factors. One method uses a ramped summation method where the higher frequency data was suppressed by the same amount that the lower frequency data was enhanced over the two-way transit time of a GPR scan. Bancroft [5] discussed this double ramped summation technique using linear or Butterworth function ramps. To determine the ramp length for each frequency, Bancroft [5] multiplied the wavelength period of a frequency by an arbitrary number of 15 for 15 wave periods. For the double ramped method two adjacent frequencies were used; one frequency that was being enhanced and one frequency that was suppressed. The ramp length was determined by the frequency that was being suppressed. The 15th wave period was used as the ramp length. The start time was determined by examining the amplitude envelope of a trace. The amplitude envelope was calculated by taking the absolute value of the Hilbert transformation of a single trace. The minimum value of the log of the averaged amplitude envelope for all traces of one frequency determines the suppression start time for that frequency.

Another method discussed was called the Amplitude Envelope Equalization (AEE) technique. Without Automatic Gain Control (AGC) applied to each frequency data set, a set of multipliers were calculated as the ratio of

the average envelope value of the lowest frequency and the average envelope value of the other frequency data sets. The weights or multipliers determined this way were applied to AGC processed frequency data sets over the portion of time that each frequency was to be enhanced. Determining the portion of time a ratio is applied was calculated by finding the minimum value of the log of the amplitude envelope (envelope computed without AGC applied); indicating the time where the suppression of that particular frequency data begins. This point was defined as data too attenuated to provide useful information. The average amplitude value of one frequency was determined by averaging the envelopes of all traces at one frequency. The weights established by this averaging method were used in conjunction with the double ramped summation method described earlier.

Bancroft [5] also suggests an alternative subjective method to determine the weighting through visual inspection of each frequency data set; but there was much less clarity as to how this was done and how experienced the reviewer must be.

Bancroft [5] process steps are as follows:

1. Clip data prior to first arrival.
2. Remove low frequency (wow).
3. Automatic gain control gain.
4. Bandpass filter.
5. Determine length of decreasing ramp in nanoseconds beginning with highest frequency.
6. Determine amplitude envelope of all traces (without AGC) of one frequency and average them. Repeat for all frequencies.
7. Determine the suppression start time by finding the minimum value of the log of the amplitude envelope.
8. Process traces adding them using the ramp summation technique.

Amplitude Envelope Equalization Technique -

1. Clip data prior to first arrival.
2. Remove low frequency (wow).
3. Automatic gain control gain.
4. Bandpass filter.
5. Determine length of decreasing ramp in nanoseconds beginning with highest frequency.
6. Determine amplitude envelope of all traces (without AGC) of one frequency and average them. Repeat for all frequencies.
7. Determine the suppression start time by finding the minimum value of the log of the amplitude envelope.
8. Determine the AEE multipliers as a ratio of the average envelope of the lowest frequency data set and the average envelope of the other frequency data sets.

9. Apply the AEE multipliers to the ramped summation technique.

IX. COMPUTER MODELING VERIFICATION

Computer model verification that GprMax delivers reasonably accurate simulated GPR scans is presented in reference [13]. In the reference, target objects were buried on a test site called "The Forest Lodge", located near Greenville, California in the Northern Sierra about 60 miles (96.56 kilometers) north of Lake Tahoe. The objects were metal (tin) roofing sheets approximately 1.83 meters (6 feet) long by 66 centimeters (26 inches) wide by 1.27 millimeters (0.05 inches) in depth. There were 8 sheets in total buried at depths of 0.5 meters (1.64 feet), 1.0 meters (3.28 feet), 1.5 meters (4.92 feet), 2.0 meters (6.56 feet), 2.75 meters (9.02 feet), 3.0 meters (9.84 feet), 3.5 meters (11.48 feet) and 4.0 meters (13.12 feet), roughly 1.83 meters (6 feet) apart. The soil content appeared to be a mixture of clay and sand, though a geological survey was not conducted. Figure 6 shows the tin sheets before burial. A MALA Imaging Radar Array System (MIRA), a multi-static radar by MALA GeoScience Corporation, was used to scan the Forest Lodge site. This radar consisted of 9 Tx's and 8 Rx's, constructed such that each receiver collected a signal from 2 adjacent transmitters at different times, constructing 2 channels received by one receiver. This radar's center frequency was set at 200 MHz providing 16 channels of data cutting a 2-meter swath over targets of interest to create a 3-D image. The results shown in Figure 7 depict only 5 of the 8 roofing sheets clearly, in a stair step fashion as they were buried. For the 3-D model of Figure 8 a dry sand medium was used for the analysis. Figure 9 and Figure 10 show two 2-D slices of the results of a 200 MHz analysis using the GprMax modeling program. Actual and model results



Figure 6. Target GPR imaging objects, tin roofing sheets, were buried at various depths. The experiments provided ground truth GPR data for hardware to software comparison.

compare favorably though the simulation shows all 8 sheets, 5 of them well. My argument that software analysis can be used successfully to study actual GPR received data is strengthened. Using a mixture of clay and sand as the medium in the model we believe would show a better fit; target reflections would be attenuated more. This could be achieved by adjusting the permittivity, affecting the velocity through the medium, and adjusting the conductivity, affecting signal attenuation. This success of actual data verses model data comparison, supports the use of computer simulation for accurate results and shall be used in the remaining analyses within this paper.

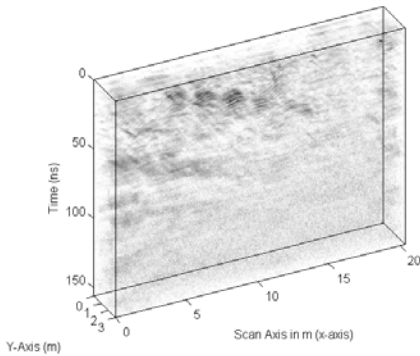


Figure 7. Processed 3-D data scanned by MALA MIRA radar over the Forest Lodge test site of buried tin sheets of known depth. 5 of the 8 roofing sheets are visible in a stair step fashion.

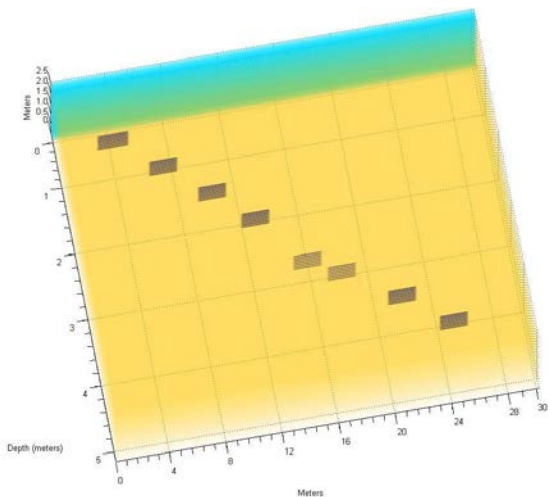


Figure 8. GprMax 3-D model of the Forest Lodge site of buried objects. This model was used to study FDTD response experiments conducted for this study.

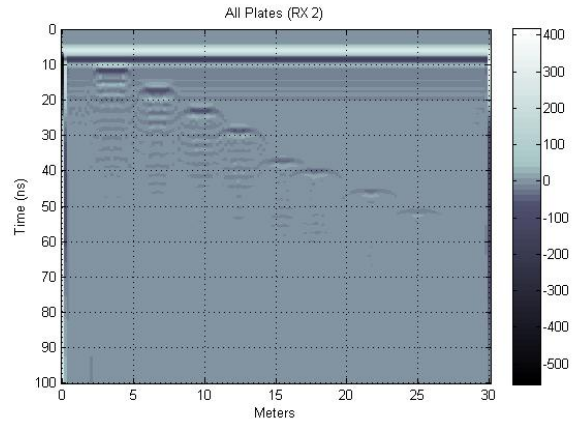


Figure 9.

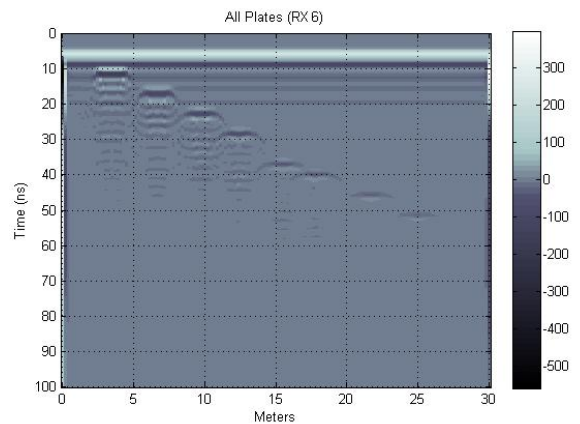


Figure 10.

Figure 9 and Figure 10 FDTD Analysis results at 200 MHz for two 2-D slices of the 3-D analysis results. All 8 of the simulated buried tin sheets are shown.

X. GPR SCAN RESULTS

To determine the capability of the EM GMM problem solver, a fictional area was defined using a Finite Difference Time Domain (FDTD) [14][15][16] modeling software package to produce GPR scans simulating real GPR scans. A Proprietary package in development, similar in operation to the popular GprMax software program by A. Giannopoulos [8] using the Transmission-Line Matrix (TLM) methods, as well as the GprMax software package were used to model a defined space. The FDTD method provides a solution to Maxwell's equations expressed in differential form. Whereas the TLM method provides a solution by simulating the propagation of electric and magnetic fields by voltage and current pulses in interconnected transmission lines [17]. Only 2-D analyses were performed.

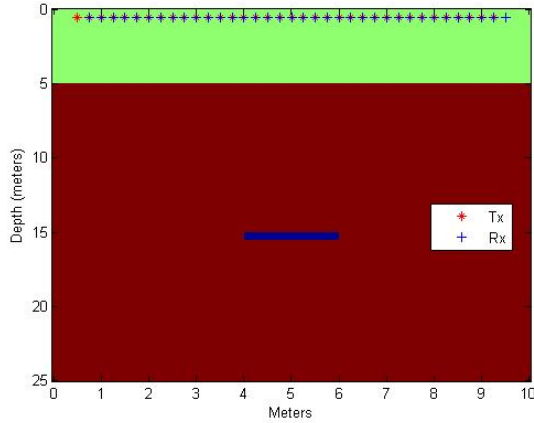


Figure 11. Defined Space with buried target at 15 meters depth and Tx's & Rx's 5 meters above ground.

The defined space modeled consisted of a Transmitter (Tx) and Receiver (Rx) suspended 5 meters above ground in air with a target (perfect electrical conductor) buried 10 meters below ground in a moist-sand medium with a relative permittivity (ϵ_r) of 9.0 and an electrical conductivity of 0.001 mS/m (Test Case 1 - TC1). The target is 2 meters in length and 0.5 meters in depth. The transmitter and receiver were moved along the length of the defined space as shown in Figure 11 for a total of 36 scans at 0.25 meters per step. The Tx starts at 0.5 meters ending at 9.5 meters, and the Rx starts at 0.75 meters ending at 9.75 meters, well within the defined space of 10 meters in length by 25 meters in depth. Each scan is 425 ns long, capable of receiving a reflected signal approximately 24 meters below Tx's and Rx's in moist-sand and air, with a minimum grid space of 200 points in x-direction, ($\Delta x = 0.05$ meters), and 500 points in y-direction, ($\Delta y = 0.05$ meters).

Simulated GPR scans were repeated for 20, 30, 50, 100, 500 and 900 MHz frequencies. A 2-D display for each frequency result is shown in Figures 12-19. In each case the object is correctly identified at approximately 10 meters below ground, approximately 15 meters below Tx's and Rx's or approximately 240 ns from the direct arrival signal (black line on plot); the two-way travel time for the radar signal. An individual trace by trace display is shown in Figure 17 and Figure 19, to better depict the target return signal. Arrow 1 in Figure 12 shows the direct arrival signal and ground bounce (radar return from the ground). Arrow 2 in Figure 12 denotes the target reflection at depth. In the 30MHz trace result (Figure 13), the target is indicated by arrow 3. The remaining unlabeled arrows indicate the target reflection at depth for the indicated scan frequency. Of interest, is the line length in frequency scans 100 MHz and below indicating the target, representing limited if not non-existent edge detection. For this analysis, the test area length is less than half the depth (25 meters depth by 10 meters length), more like a bore hole, contributing to the limited target edge detection. Arrow 4 (Figure 19) exhibits better edge detection.

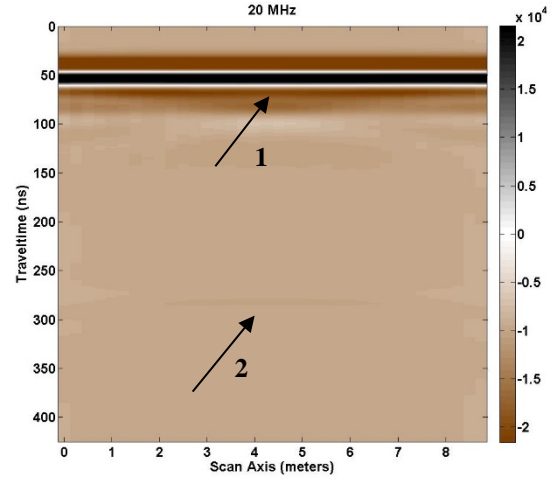


Figure 12. 2-D GPR scans 20MHz.

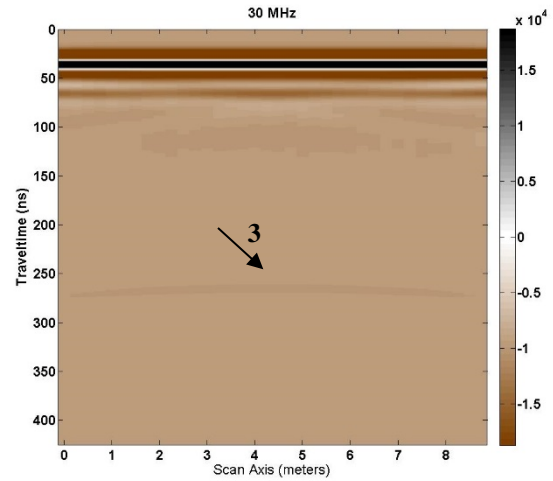


Figure 13. 2-D GPR scan 30MHz.

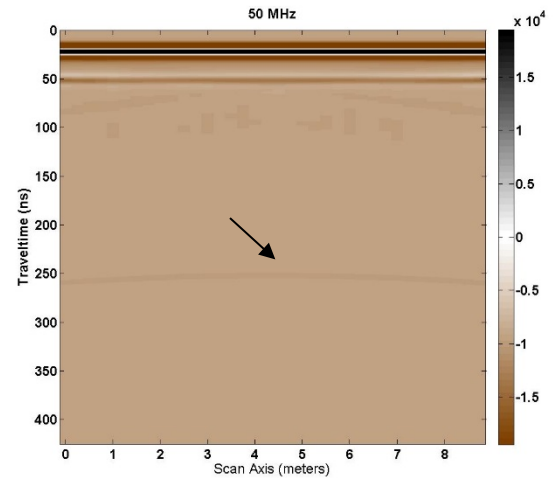


Figure 14. 2-D GPR scan 50MHz.

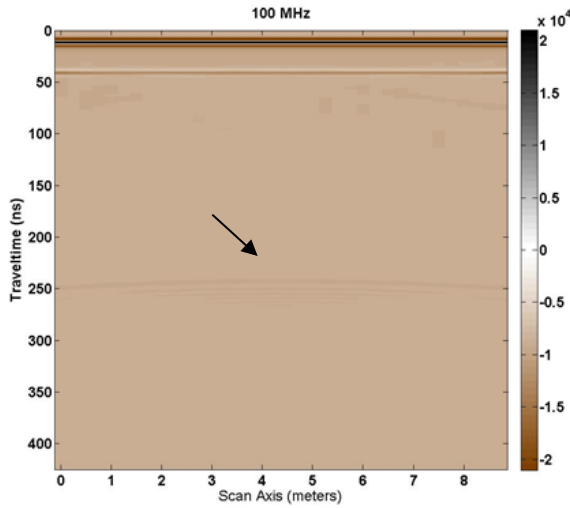


Figure 15. 2-D GPR scan 100MHz.

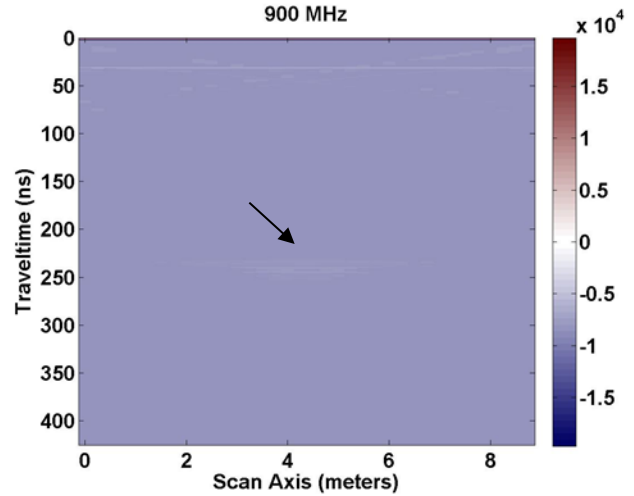


Figure 18. GPR scan 900MHz (normal 2 D image display).

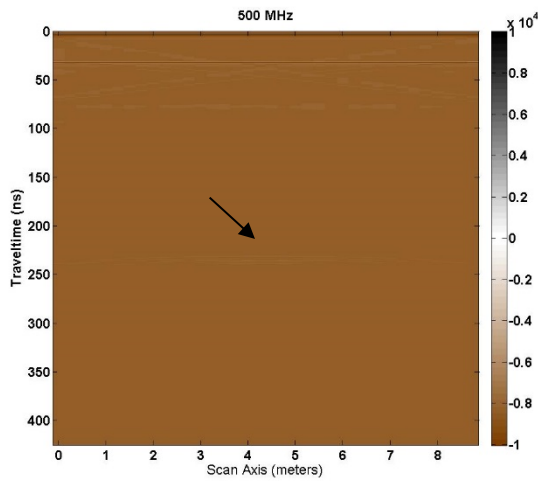


Figure 16. GPR scan 500MHz.

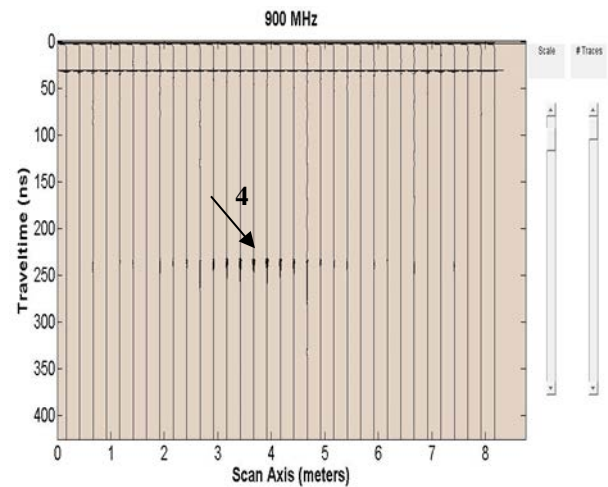


Figure 19. GPR scan 900MHz (individual traces).

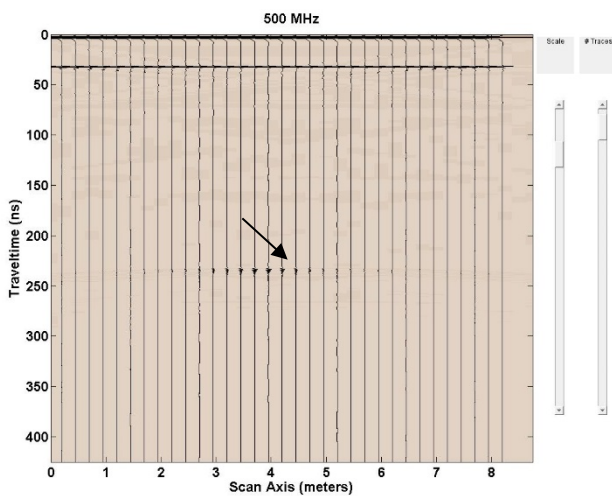


Figure 17. GPR scan 500MHz (individual traces).

In all the simulated GPR scan results, as the frequency is increased, the area where the target exists is more pronounced. The opposite occurs as the scan frequency is lowered.

Figure 20 shows the result of adding each of the frequencies together having removed the direct arrival signal and scaling each signal max value to the same magnitude. A broad area of target reflection is shown from approximately 240 ns to 320 ns in depth (two-way travel time); a very rough indication of target depth. The direct arrival signal was removed by subtracting a GPR scan without a target from a scan with a target, for each frequency.

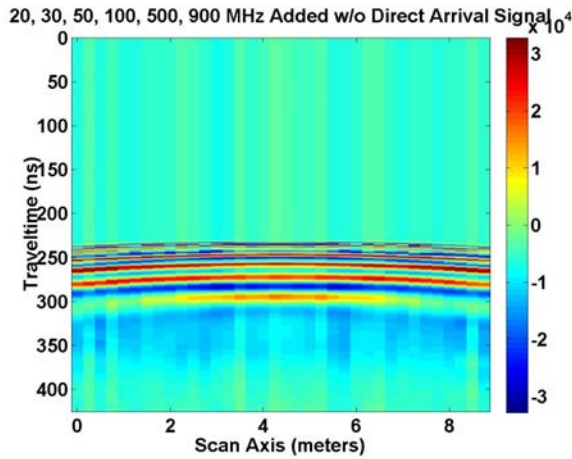


Figure 20. Sum of frequency signals with direct arrival and ground bounce signals removed.

Figure 21 and Figure 22 show the same signals combined using the EM algorithm to determine the weight of each signal. Figure 22 shows the EM processed individual signal traces. The area that is being scanned is more like a bore hole, twice as deep as its width. This accounts for the broad reverse “u-shaped” area that begins at target depth. The existence of lower frequencies in the sum broadens the output result.

Figure 23 shows the results of applying the Dougherty et al. [3] approach to the same test area. The target depth is correctly identified but the depth indication is slightly less crisp than the EM algorithm case. The EM case depicts a thinner line in depth. It appears the delta depth issue (less crisp) is the result of the lower frequencies in the sum.

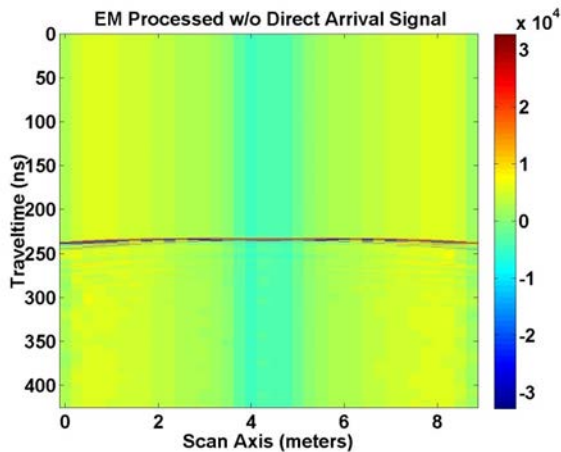


Figure 21. EM sum of frequency signals with Direct Arrival and ground bounce signals removed.

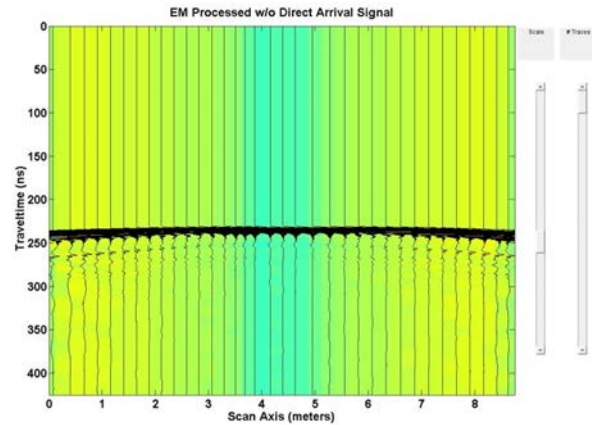


Figure 22. EM processed signal traces with Direct Arrival and ground bounce signals removed.

However, the Dougherty et al. [3] approach shows better edge detection. The width of the target is better defined though still wider than the defined area but less than the EM GMM case. For the Dougherty et al. [3] case, part of the Direct Arrival/Ground bounce signal is visible due to the method used to remove them from each frequency scan.

For the same test area, applying the Booth et al. [4] OSW approach with one time-window results in the output shown in Figure 24. Again, the target depth is correctly identified but like the Dougherty et al. [3] method the depth indication is quite broad. The delta time depth indication is larger than the EM and Dougherty et al. [3] methods, (Figure 21 and Figure 23). Similar to the EM method, the width in scan axis length is large; edge detection is not well defined. The thickest part of the trace indicates the test target.

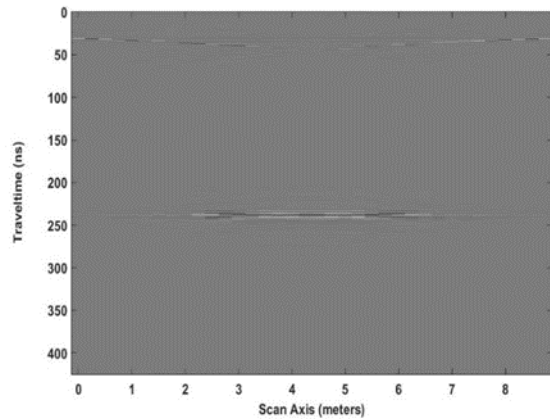


Figure 23. Dougherty et al. [3] standard response for TC1.

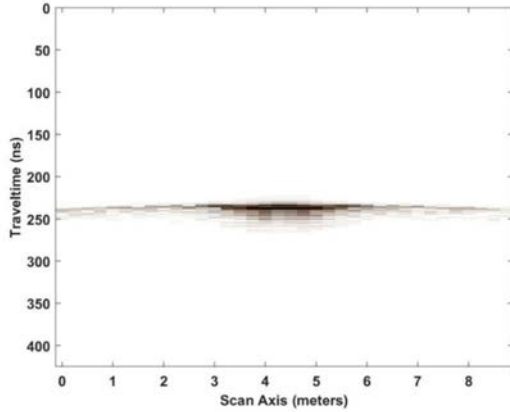


Figure 24. Booth et al. [4] response for TC1.

Figure 25 demonstrates the AEE method of Bancroft [5]. The target depth is correctly identified and the depth indication is like that of the EM method, sharp but slightly broader in depth. This is about the same as the Dougherty et al. [3] method, and smaller than the Booth et al. [4] method. Target edge detection is more like Booth et al. [4] where the thickest part of the GPR result indicates the test target. Like the EM method the GPR reflection covers a wide area (0 to 9 meters) in scan axis length. How much of this response is due to the bore hole effect of the target area is unknown at this time. We applied a modified AEE method consisting of calculated multipliers only and not the ramped summation because the calculated start and end of each ramp conflicted with each other, which is not the case for the scan frequencies chosen by Bancroft [5].

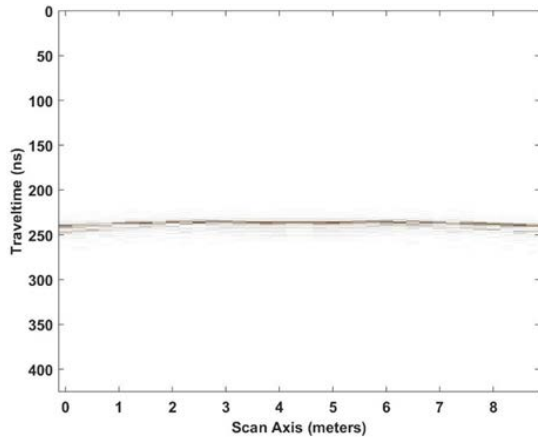


Figure 25. Output from Amplitude Envelope Equalization method of Bancroft [5] for TC1.

For test case 1, the test area definition poses a problem as to the effect of the bore hole like definition of the target area, on the outcome of the scan response. Of concern, is whether a less than crisp edge detection or the addition of large magnitude lower frequencies, are making the depth indicators broad. By exercising a more complicated test area

with broader scan area we attempted to address these concerns.

The second defined area consists of an area 30 meters in length and 25 meters in depth with little or no space above ground, (0.15 meters), for the Tx and Rx used (Test Case 2 – TC2). They are swept along the scan axis length starting at 0.5 meters (Tx) and ending at 24.85 meters with spacing between the Tx and Rx the same as before (0.25 meters), as shown in Figure 26. The number of GPR scans is 145. The electrical conductivity of the ground is the same as before but the relative permittivity (ϵ_r) is 3.0 for dry sand. Each scan is 550 ns long, capable of receiving a reflected signal approximately 48 meters below Tx’s and Rx’s in dry sand, with a minimum grid space of 150 points in x direction, (Δx – 0.2 meters), and 2500 points in the y direction, (Δy - 0.01 meters). Simulated burial in the ground at 8 different levels (4.565, 6.065, 8.565, 10.065, 12.815, 14.065, 16.565 and 18.065 meters) are sheets of corrugated aluminum, modeled as perfect electrical conductors for ease of computation. Each sheet is approximately 2 meters in length and 0.1 meters in depth. The GPR scanning frequencies are the same as before. The result for the EM method, shown in Figure 27, identifies 8 targets at very close to the correct depth (approximately 50, 70, 100, 116, 148, 160, 190 and 208 ns for two-way travel time at a velocity in the medium of 0.1732 m/ns for the defined relative permittivity) with edges depicted reliably but with less fidelity as one descends in depth. Figure 28 displays the individual GPR traces instead of the image response.

Applying the Dougherty et al. [3] method to this second test area produces the GPR response shown in Figure 29. Note that not all plates are depicted. Only 5 and barely 6 of the 8 are designated. Where the plates end in width is tolerably detectable; edges are noted but not clearly. The result is poorer than the EM processed response of Figure 27; direct arrival signal removed by subtraction as before.

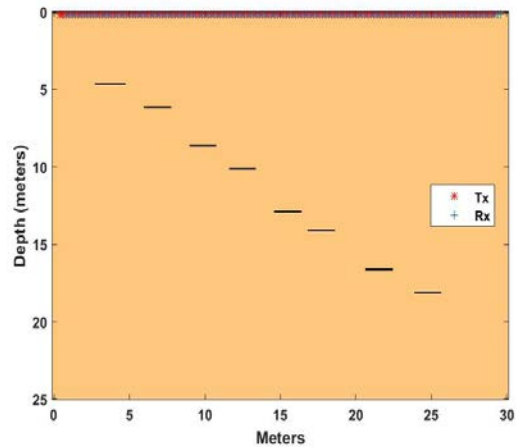


Figure 26. EM algorithm Test Case, (8) 2 meter long plates, 0.1 meter thick.

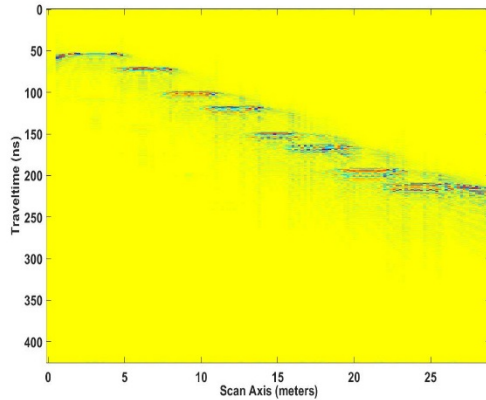


Figure 27. GPR scan result for complex structure.

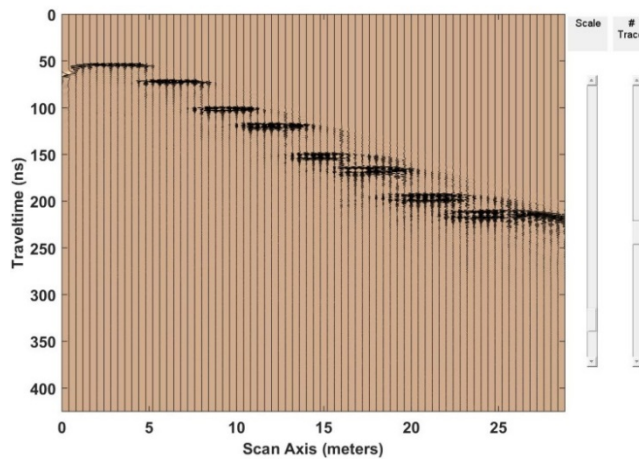


Figure 28. EM processed signal traces for complex structure.

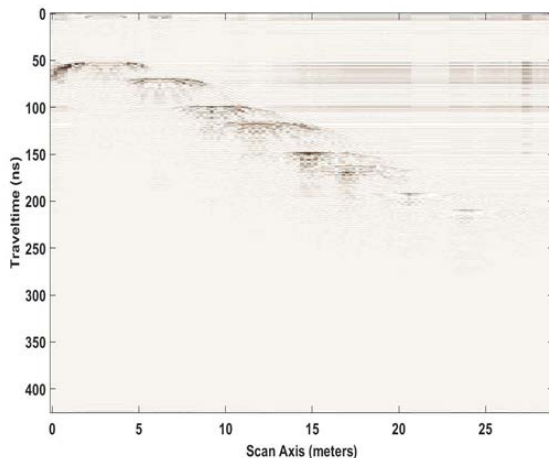


Figure 29. Dougherty et al. [3] standard response for TC2.

Figure 30 shows the GPR response of the Booth et al. [4] OSW method with one time-window applied to this second test area. The ground bounce (shown as a straight line at approximately 50 ns in Figure 30) is still present in the

image because the mute feature had to balance between removing the direct arrival/ground bounce signal and not removing the reflection of the first plate at a depth of approximately 50 ns two-way travel time. Again only a few plates are detectable. Easily shown are the first 4 plates and barely plates 5 and 6 of the 8 plates in the test area. Comparing the result to the EM method, the Booth et al. [4] method falls short at depth. Edge detection is poorer than the EM method but comparable to the Dougherty et al. [3] method.

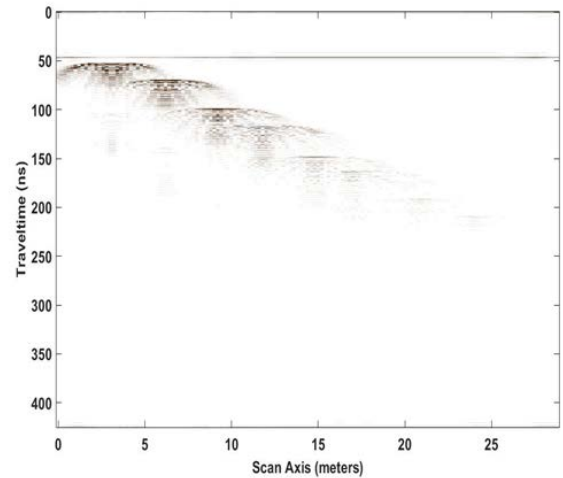


Figure 30. Booth et al. [4] response for TC2.

Figure 31 depicts the result of employing the AEE Bancroft [5] method on test area 2. Like Booth et al. [4] and Dougherty et al. [3] before, not all buried plates are illuminated. Of the 8 plates, 4 are depicted with a possibility of 3 more. Added under plates at 50 ns and 75 ns in depth are “ghost” plates at 100 ns and 150 ns. There were no targets buried at these two points. Edge detection is better than Booth et al. [4] and Dougherty et al. [3] and on par with the EM algorithm. Again, only the calculated AEE multipliers were used due to the same ramp start and end conflict issue.

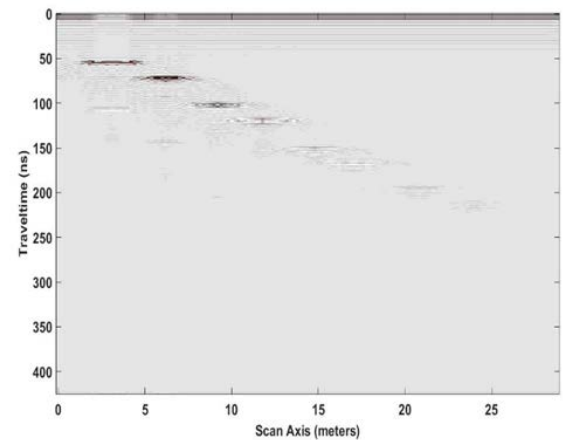


Figure 31. Bancroft [5] response for TC2.

For this more complicated test case, the EM algorithm has performed the best in terms of revealing the 8 buried plates. Edge detection is still not great but tolerable for the EM method for both test cases and the Bancroft method for the second test case. The larger scan area does address the bore hole effect question of wider scan axis length reducing wide reflection traces. The dimensions of the scan area does affect the width of the scan axis reflections. The ability to achieve crisp edge detection has not changed much however.

The previous test cases modeled were all in homogenous material either moist sand or dry sand. Of interest to be modeled were objects placed in a non-homogenous material; layered like what could appear in nature. As an additional test case (TC3), a model area was created with dry sand, clay, concrete, granite, and limestone with relative permittivity of material noted in Figure 32. Sheets of corrugated aluminum, modeled as perfect electrical conductors were buried as noted in the previous test case. The result (Figure 33) for the EM method on this test case mirrors that of the previous homogeneous medium case. There are a few subtle changes (coloration differences – the concrete buried object, plate 6, has a lighter color for example), which coincide with material the aluminum sheets (perfect electrical conductors) are buried in. Figure 34 shows the individual GPR traces.

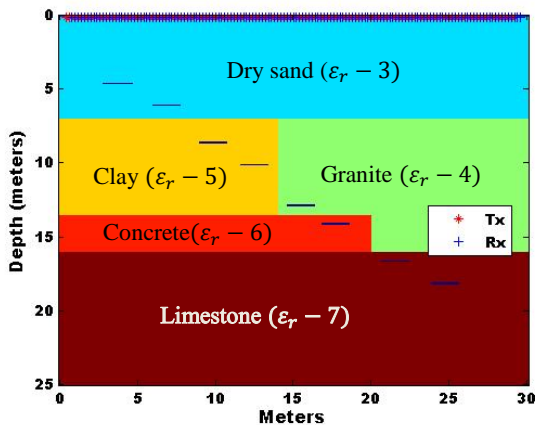


Figure 32. Test Case Area 3 (8) 2 meter long plates, 0.1 meter in depth.

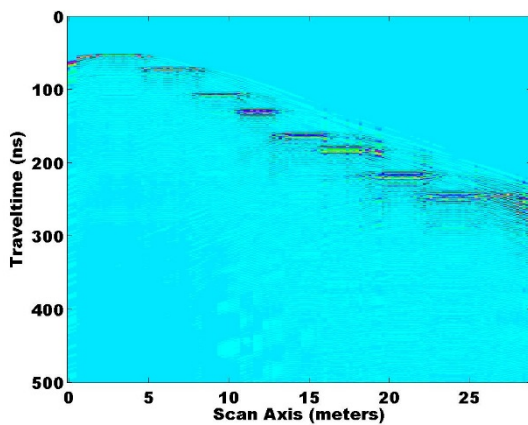


Figure 33. EM Algorithm GPR scan result for TC3 (8) Plates shown

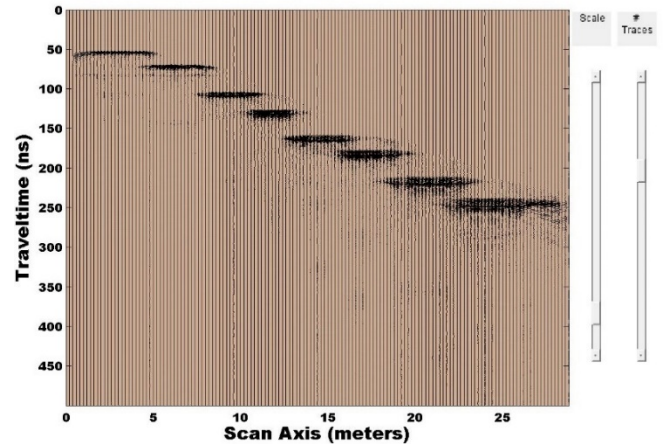


Figure 34. EM Algorithm GPR Scan result showing individual traces for TC3.

XI. CONCLUSION AND FUTURE WORK

In this paper, we have explored using the Expectation Maximization Gaussian Mixture Model, an optimization problem solver, to define weights to combine multiple GPR frequency scans over the same area to improve image resolution to a lower depth. First, we looked at using the EM GMM method to combine multiple frequency sine waves to form a square wave by defining the best set of weights for the square wave frequency harmonics presented. Though not without problems, the process performs reasonably well in forming a square wave combining the multiple frequencies. The value of the mixture weights summing to one is an issue to look at; but they are defined that way in the EM GMM algorithm. Actual multiple sine wave mixture weight values are different but similar in magnitude. Though not ideal, there was enough success to pursue using the EM GMM technique on GPR scans over the same area at different frequencies, the first use of this technique on GPR scans of multiple frequencies. We explored whether the Maximum Likelihood Estimation process would be more fitting for our analyses. In exploring this technique, we were reminded that the MLE process, though workable, presents problems when hidden or incomplete data exists [6][7]. The resultant likelihood equation does not have a closed form solution or a single global maximum and becomes very hard to solve. Whereas the EM Algorithm provides a well-structured solution by creating a set of simpler optimization sub-problems, from the MLE process, that are guaranteed to converge and produce local maxima at each iteration that increase until a global maximum is reached.

In considering the EM GMM case for GPR signals we encountered several other methods, in the literature, that attempted to combine scans of various frequencies over the same target area. Methods by Dougherty et al. [3], Booth et al. [4] and Bancroft [5] were compared to our EM GMM method [18] as a way to judge how well our method performed compared to solutions found in the literature. Because we lacked the equipment hardware to perform field

experiments, a well-known computer program was used to model simulated target areas. The targets were perfect electrical conductors and the media used well-defined permittivity values. The scan results demonstrated the effectiveness of the software program GprMax [8]. The connection between actual and simulated results were detailed in reference [13] and discussed here briefly. The GprMax [8] results were determined to be an accurate depiction of field experiments. We found that in comparing our EM GMM process with Dougherty et al. [3], Booth et al. [4] and Bancroft [5], our process fared the best in recognizing images at depths down to 20 meters in moist sand and dry sand media. As a final test, we performed an experiment with the same targets positioned this time in several media types that varied with depth from the surface. In this non-homogenous experiment, we used dry sand first then, clay and granite, concrete and finally limestone as the final layer. The result was the same as without such division in media types.

Our results uncovered problem areas in need of future study. The edge detection ability, how to reliably remove the direct wave/ground bounce without removing the reflected radar response from the target, and how to best align GPR trace starting points across frequencies, are a few examples. Solving the alignment problem appears to reduce the thickness in depth of the GPR scan results. Of interest in a future project would be the result of using the EM GMM method in finding tunnels in a realistic clutter environment.

APPENDIX A

A.1 GPR BASICS

Ground Penetrating Radar method provides a way to map sub-surface artifacts or structures using radio waves. GPR modes in practice consist of reflection, velocity sounding (common mid-point) mode and trans-illumination. The most common mode is the reflection mode where a GPR radio wave from a transmitter at or above the ground surface, propagates through a medium to a buried target, reflecting the radar wave back to a receiving antenna. The velocity sounding or common mid-point mode provides a method to determine the velocity of the radio wave in a medium by setting a transmitter and receiver at a specified distance apart; instituting a scan then, moving both transmitter and receiver a distance further apart, repeating the process several times. The result provides a way to calculate the velocity through the medium that the radio waves have encountered. Trans-illumination is used for Bore holes in two ways; One, a transmitter (Tx) and receiver (Rx) are moved in unison from one position to another beginning at the surface of a bore hole then, lower on either side of the area of interest; scanning is across the area of interest. Two, only one transmitter is used and several receivers are placed at various positions in depth. Figure 1A depicts these modes. Antenna orientation, polarization and the available power verses the loss mechanisms determined

by the radar range equation are of interest but beyond the scope of this paper.

Of interest in the reflection mode method are the signal arrival types, the theoretical resolution of a GPR system, and what item is the major contributor to the velocity in a medium. The signal arrival types are the direct air wave, critically refracted air wave, direct ground wave, and reflected wave. The theoretical resolution is proportional to $\frac{1}{4}$ of the velocity in a medium divided by the frequency of the radio wave (i.e. the wavelength in a medium divided by 4; *Theoretical resolution* = $(\lambda = \frac{v}{f})/4$). The velocity in a medium is proportional to the speed of light in a vacuum divided by the square root of the relative permittivity of the medium making permittivity the major influence on the velocity in a medium.

$$Velocity = (c/\sqrt{\epsilon_r}) * 1e^{-9} \text{meters/ns} \quad (1A)$$

c = speed of light ($3e^8$ meters/sec)
 ϵ_r – relative permittivity

Permittivity is defined as a measure of how an electric field is affected and affects a dielectric medium. Figure 2A and Figure 3A. depict the signal arrival types, and equations governing time, depth and velocity measurements.

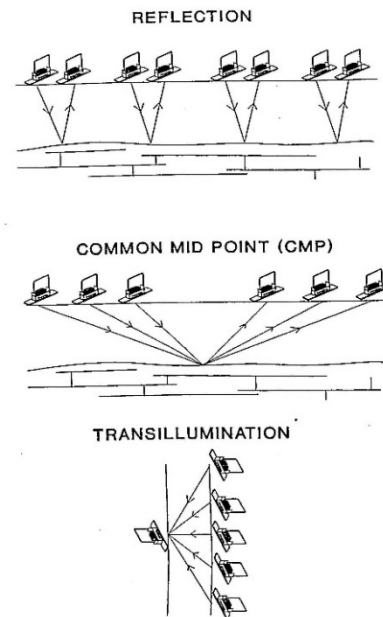


Figure 1A. GPR Scanning Modes [19].

Typically, short radar pulses are transmitted into the medium. The most common pulses used are the “Ricker Pulse” (second derivative of a Gaussian pulse) or the first derivative of a Gaussian pulse (a Monocycle) (Figure 4A).

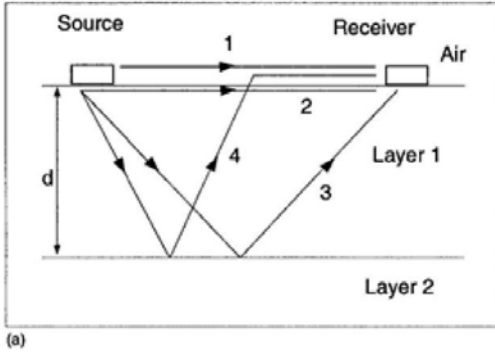


Figure 2A. GPR Arrival Types [20].

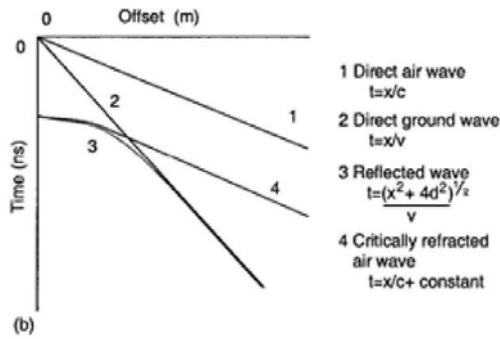


Figure 3A. Simple CMP plot w/equations for Arrival Types [20].

Most equipment manufacturers do not divulge their transmit pulse type; but the “Ricker” Pulse is assumed. Figures 5A-8A show plots of typical reflected signals received without a buried target at various frequencies. Each Tx/Rx is 5 meters above the ground (dry sand) in air. Shown are the direct arrival signal and the ground bounce. Note as the frequency increases, the direct arrival gets sharper and the ground bounce is better defined though the time of the return signal occurs is the same.

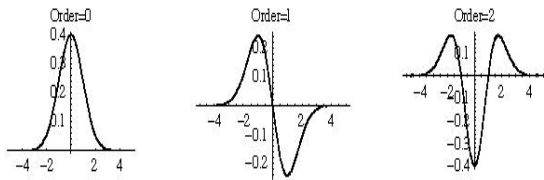


Figure 4A. Gaussian, 1st derivative (Monocycle), 2nd derivative (Ricker)(normally GPR response signals for Monocycle and Ricker are inverted) [21].

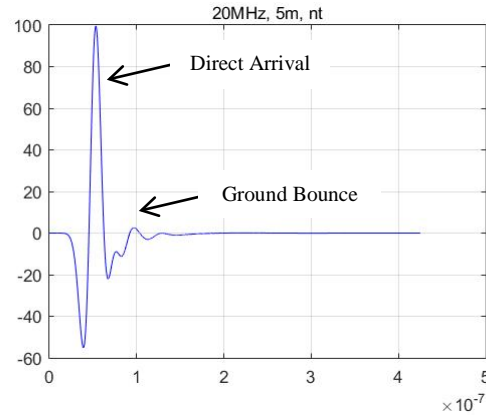


Figure 5A. Direct arrival and ground bounce, 20MHz.

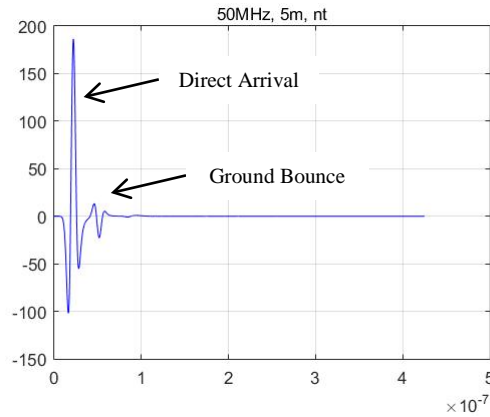


Figure 6A. Direct arrival and ground bounce, 50MHz.

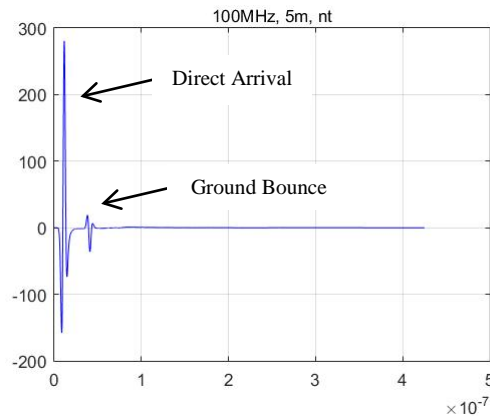


Figure 7A. Direct arrival and ground bounce, 100MHz.

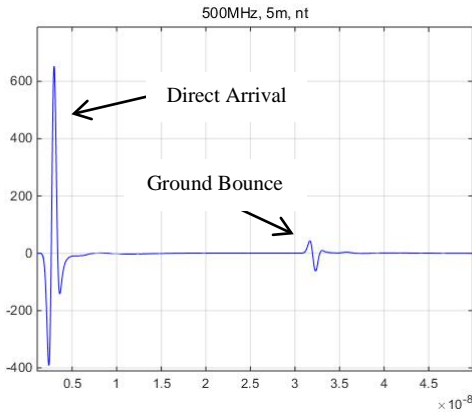
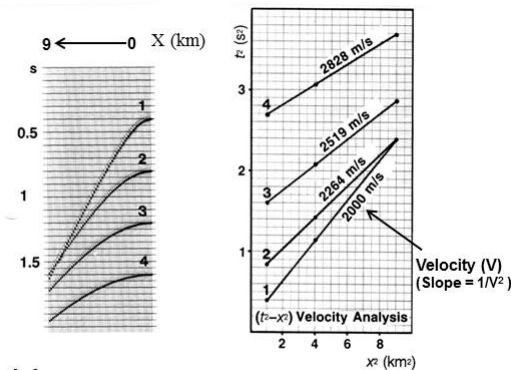


Figure 8A. Direct arrival and ground bounce, 500MHz.

Several methods exist to calculate the velocity of a radio wave in a medium. The two most popular are derived from the common mid-point (CMP) mode. Figure 3A depicts the first method, a simple plot of the CMP results with equations. Figure 9A depicts the second method, the (time² - Tx/Rx separation²) analysis method named (t²-x²) where the slope of the plot is equal to 1/(velocity squared). With simple manipulation of the result, the velocity in a medium can be determined.



Example of a t²-x²-Analysis.

Figure 9A. Shows t² - x² Analysis (s ↔ t) [22].

A.2 MODELING BASICS

The top 2 methods used to model GPR analysis are the Transmission-Line Matrix (TLM) method and the Finite Difference Time Domain (FDTD) method [15]. Both methods provide a solution to Maxwell's equation subject to geometry, initial conditions, and boundaries of a problem. The TLM method [17] is implemented as an electrical network model solution to an electromagnetic field problem. Transmission lines are interconnected at regular intervals to form TLM nodes. The propagation of electric and magnetic fields are simulated by voltage and current pulses. The model space step defines the distance between TLM

adjacent nodes. The time step represents the time, which a pulse takes to travel from one TLM node to the next.

The FDTD method provides a solution to Maxwell's equations expressed in differential form. The partial derivatives in Maxwell equations are discretized using central difference techniques resulting in difference equations, which are solved by an iterative process. Included in the difference equations are the model space step and time step.

A.3 TWO-WAY-TRAVEL-TIME (TWTT)

Figure 10A and Figure 11A demonstrate the GPR trace of the example in Figure 6 at 20 and 50 Mhz. The target is 10 meters below the ground and 15 meters from the Tx's and Rx's. There are 2 mediums the radar signal travels through, free space (Tx/Rx to ground) and moist sand (ground to target). The velocities for the 2 mediums are 0.3 m/ns (free space) and 0.1 m/ns (moist sand). To determine the distance to the target from the Tx/Rx from Figure 7A, the mediums and the velocity through the mediums along the following occurs.

$$TWTT = \frac{2 * distance \text{ Tx/Rx to target}}{Velocity \text{ through the media}} \quad (2A)$$

TWTT = 280 ns - 40 ns = 240 ns, from Figure 7A.

Medium 1 - free space, velocity 0.3 m/ns, distance to ground from Tx/Rx is 5 meters

$$TWTT(1) = (2 * 5 \text{ meters}) / (0.3 \text{ m/ns}) \approx 33 \text{ ns}$$

Medium 2 - moist sand, velocity 0.1 m/ns, distance to target from ground is:

$$d = (0.1 \text{ m/ns} * (240 \text{ ns} - 33 \text{ ns})) / 2 \approx 10.35 \text{ meters.}$$

Total calculated distance (d) from Tx/Rx to target is 15.35 meters (5 meters + 10.35 meters); close to the defined 15-meter distance, but accurate because true distance from Tx/Rx to target is at an angle, which is longer than the perpendicular distance.

A.4 VELOCITY THROUGH A MEDIUM AND PENETRATION DEPTH [23]

The velocity is dependent on a material's relative permittivity. The higher the relative permittivity of a medium, the lower the velocity is through the medium. When the relative permittivity of a medium is known the calculated velocity through the medium can be calculated using equation 1A.

Example: free-space has a permittivity (ε_r) = 1,
 $Velocity = [3e + 8 / \text{Sqrt}(1) * 1e - 9] \text{ m/ns.}$
 $V = 0.3 \text{ m/ns.}$

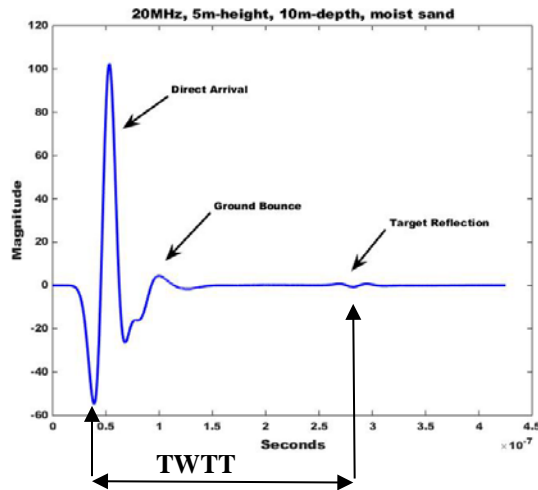


Figure 10A. GPR trace depicting Two-way-transit-time for a target at 20MHz.

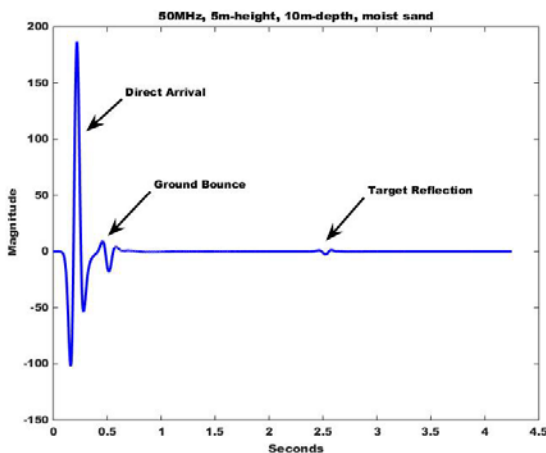


Figure 11A. GPR trace depicting Two-way-transit-time for same target of Figure 10A at 50 MHz.

As the electrical conductivity, (units Siemens/meter), increases the penetration depth decreases, determining how deep an electrical signal will penetrate. Higher frequencies reduce the depth penetration but increase image resolution. Table 1 lists a few nominal values for permittivity and conductivity.

TABLE 1 (MEDIUM AND VELOCITY VALUES)

| Medium | ϵ_r | Velocity (m/ns) | Conductivity (mS/m) |
|-----------|--------------|-----------------|---------------------|
| concrete | 6 | 0.1225 | 0.01 |
| clay | 5 | 0.1342 | 2 |
| dry-sand | 3 | 0.1732 | 0.01 |
| granite | 4 | 0.1500 | 0.01 |
| limestone | 7 | 0.1134 | 0.5 |

ACKNOWLEDGMENT

This work was performed under the auspices of Sandia National Laboratories a multimission laboratory managed and operated by National Technology and Engineering Solutions of Sandia, LLC, a wholly owned subsidiary of Honeywell International, Inc. for the U.S. Department of Energy’s National Nuclear Security Administration under contract DE-NA-0003525.

REFERENCES

- [1] R. Tilley, H. Sadjadpour, and F. Dowla, “Combining Ground Penetrating Radar Scans of Differing Frequencies Through Signal Processing,” The Ninth International Conference on Advanced Geographic Information Systems, Applications, and Services, GEOProcessing 2017, Nice, France, Mar 2017, pp. 32-38, ISBN:978-1-61208-539-5.
- [2] A. L. Endres, A. Booth, and T. Murray, “Multiple Frequency Compositing of Spatially Coincident GPR Data Sets,” Proceedings of the Tenth International Conference on Ground Penetrating Radar, 2004, Delft, The Netherlands, June 2004, pp. 271-274, ISBN: 90-9017959-3.
- [3] M. E. Dougherty, P. Michaels, J. R. Pelton, and L. M. Liberty, “Enhancement of Ground Penetrating Radar Data Through Signal Processing,” Symposium on the Application of Geophysics to Engineering and Environmental Problems 1994, pp. 1021-1028, Jan 1994, DOI 10.4133/1.2922053.
- [4] A. D. Booth, A. L. Endres, and T. Murray, “Spectral Bandwidth Enhancement of GPR Profiling Data Using Multiple-Frequency Compositing,” Journal of Applied Geophysics, vol 67, pp. 88-97, Jan 2009, DOI 10.1016/j.japge.2008.09.015.
- [5] S. W. Bancroft, “Optimizing the Imaging of Multiple Frequency GPR Datasets using composite Radargrams: An Example from Santa Rosa Island, Florida,” PhD dissertation, University of South Florida, 2010.
- [6] A. P. Dempster, N.M. Laird and D.B. Rubin, “Maximum Likelihood from Incomplete Data via the EM Algorithm,” Journal of the Royal Statistical society, Series B (Methodological) 39(1): pp. 1-38, 1977, JSTOR 2984875.MR0501537.
- [7] C. R. Shalizi, “Advanced Data Analysis from an Elementary Point of View,” Book Draft from Lecture Notes for Course 36-402 at Carnegie Mellon University, Chapters 19.1-19.2.2, January 2017, <http://www.stat.cmu.edu/~cshalizi/ADAfaEPoV/ADAfaEPoV.pdf>, 2017.11.23.
- [8] A. Giannopoulos, “Modelling Ground Penetrating Radar by GprMax,” Construction and Building Materials, vol. 19, pp. 755-762, Dec 2005, DOI 10.1016/j.conbuildmat.2005.06.007.
- [9] J. A. Pena, T. Teixido, “Cover Surfaces as a New Technique for 3-D Image Enhancement, Archaeological Applications,” Repositorio Institucional de la Universidad de Granada, Spain, 2012, <http://hdl.handle.net/10481/22949>, 2017.11.23.
- [10] Padhraic Smyth, “The EM Algorithm for Gaussian Mixtures, Probabilistic Learning: Theory and Algorithms, CS274A,” University of California, Irvine, Department of Computer Science, Lecture Note 4.
- [11] J. J. Verbeek, N. Vlassis, and B. Kröse, “Efficient Greedy Learning of Gaussian Mixtures,” The 13th Belgian-Dutch Conference on Artificial Intelligence (BNAIC’01),pp. 251-258, 2001, INRIA-00321510.

- [12] C. Do, S. Batzoglou, "What is the Expectation Maximization Algorithm," *Nature Biotechnology* vol. 26, Issue 8, pp. 897-899, 2008, DOI 10.1038/NTBL1406.
- [13] R. Tilley, F. Dowla, F. Nekoogar, and H. Sadjadpour, "GPR Imaging for Deeply Buried Objects: A comparative Study based on FDTD models and Field Experiments," *Selected Papers Presented at MODSIM World 2011 Conference and Expo*; pp. 45-51, Mar. 2012; (NASA/CP-2012-217326); (SEE 20130008625).
- [14] A. P. Annan, "Electromagnetic Principles of Ground Penetrating Radar," in *Ground Penetrating Radar Theory and Applications*, M. J. Harry, Ed., ed Amsterdam: Elsevier, pp. 1-40, 2009, ISBN: 978-0-444-53348-7.
- [15] A. Tavlove, "Review of the formulation and Applications of the Finite-Difference Time-Domain Method for Numerical Modeling of Electromagnetic-Wave Interactions with Arbitrary Structures," *Wave Motion*, vol. 10, pp. 547-582, Dec 1988, DOI 10.1016/0165-2125(88)90012-1.
- [16] N. Blindow, D. Eisenburger, B. Illich, H. Petzold, and T. Richter, "Ground Penetrating Radar," in *Environmental Geology*, Ed. Springer Berlin Heidelberg, pp. 283-235, 2008, DOI 10.1007/978-3-540-74671-3_10.
- [17] C. Christopoulos, "The Transmission-Line Modeling (TLM) Method in Electromagnetics," *Synthesis Lectures on Computational Electromagnetics*, vol. 1, Issue 1, pp. 1-132, Morgan & Claypool Publishers, 2006, DOI 10.2200/S00027ED1V01Y200605CEM1007.
- [18] R. Tilley, H. Sadjadpour, and F. Dowla, "Extending Ground Penetrating Radar Imaging Capabilities Through Signal Processing," *Proceedings of the 2nd World Congress on Civil, Structural, and Environmental Engineering (CSEE'17)*, Barcelona, Spain, April 2017, ISSN 2371-5294, DOI 10.11159/icgre17.194.
- [19] A. P. Annan, and S.W. Cosway, "Ground Penetrating Radar Design," *Proceedings of the Symposium on the Application of Geophysics to Engineering and Environmental Problems (SAGEEP)*, vol 2, pp. 329-351, 1992, DOI 10.4133/1.2921946.
- [20] J. van der Kruk, E. C. Slob, and J. T. Fokkema, "Background of ground-penetrating radar measurements," *Journal of Geologie en Mijnbouw*, vol. 77, Issue 2, pp. 177-188, 1998, DOI 10.1023/A:103546619639.
- [21] B. M. ter Haar Romeny, "Front-End Vision and Multi-Scale Image Analysis: Multi-Scale Computer Vision Theory and Applications written in Mathematica," Springer Publishers, 2008, ISBN 978-1-4020-1507-6.
- [22] J. van der Kruk, "Reflection Seismic I," *Lecture Series in WS 2004/2005*, Institut für Geophysik ETH Zürich, http://www.wgeosoft.ch/Document/Reflection_ETHZ.pdf, 2017.11.23.
- [23] H. M. Jol, editor, "Ground Penetrating Radar Theory and Applications," Elsevier Science, 2009, ISBN: 978-0-444-53348-7.